Influence of microstructural heterogeneity on the scaling between flow stress and relative density in microcellular Al-4.5%Cu

Yves Conde*, Roberto Doglione**, and Andreas Mortensen

Ecole Polytechnique Fédérale de Lausanne, Institut des Matériaux
Laboratoire de Métallurgie Mécanique,
Station 12, CH- 1015 Lausanne, Switzerland

* Corresponding author, now with Constellium
EPFL - Quartier de l'Innovation, Bâtiment E, CH-1015 Lausanne, Switzerland

**INSTM, via G. Giusti 9, 50121 Firenze, Italy.

JOURNAL OF MATERIALS SCIENCE

IN PRINT

ABSTRACT

We explore the influence of the metal microstructure on the compressive flow stress of replicated microcellular 400 μm pore size Al-4.5wt%Cu solidified at two different solidification cooling rates, in as-cast and T6 conditions. It is found that the yield strength roughly doubles with age-hardening but does not depend on the solidification cooling rate. Internal damage accumulation, measured by monitoring the rate of stiffness loss with strain, is similar across the four microstructures explored and equals that measured in similar microcellular pure aluminium. *In-situ* flow curves of the metal within the open-pore microcellular material are back-calculated using the Variational Estimate of Ponte Castañeda and Suquet. Consistent results are obtained with heat-treated microcellular Al-4.5wt%Cu, and are also obtained with separate data for pure Al; however, for as-cast microcellular Al-4.5wt%Cu the back-calculated *in-situ* metal flow stress decreases, for both solidification rates, with decreasing relative density of the foam. We attribute this effect to an interplay between microstructural and mesostructural features of the microcellular material: variations in the latter with the former held constant can alter the scaling between flow stress and relative density within microcellular alloys.

Keywords: cellular materials, deformation and fracture, porosity, replication processing

1. INTRODUCTION

Replicated microcellular aluminium is made by producing a porous preform of bonded NaCl powder for subsequent infiltration with aluminium or one of its alloys [1, 2]. After metal solidification, the NaCl preform is removed by dissolution in water to create a fine interconnected network of metal. The packed NaCl particle bed gives pores of the material their shape, or in other words defines the microcellular material's *mesostructure*. Its *microstructure* is, on the other hand, defined by the alloy composition, and by internal features of its constituent metal or alloy.

Both the mesostructure and the microstructure are known to influence the properties of microcellular metals or alloys; general reviews of structure/property relations in those materials can be found in Refs. [2-4]. At high porosity, the influence of the mesostructure is dominant: variations in the architecture of microcellular metal can change their general load-bearing capacity in both elastic or plastic deformation by several orders of magnitude (for illustration of this see Figs. 17 and 18 of Ref. [5] and Figs. 5 to 7 of Ref. [6]). The microstructure, on the other hand, exerts its influence by changing intrinsic properties of the solid metal or alloy making the microcellular material at hand. Microstructure variations will thus generally not change dramatically the elastic modulus of microcellular metals (since the stiffness of most engineering alloys is relatively insensitive to microstructure or composition) but will influence the strength of microcellular metals significantly, *a priori* in equal proportion to what is observed in dense metals and alloys. This is for example visible in the fact that significant increases in flow stress can be produced in microcellular metals by heat-treatment if their constituent metal alloy is an age-hardening alloy [7-18]. Harnessing the microstructure of microcellular metals is thus an interesting way of optimizing their strength.

A question this raises is whether processing-microstructure-strength relations remain the same, in microcellular metals or alloys, as in the same metal or alloy when it is dense. Often, this is not so: Thornton and Magee showed in their pioneering study of aluminium foams [19], as did Yamada et al. for microcellular magnesium alloys [20, 21], that heat treatment can affect the foam very differently than it does the bulk alloy; 6xxx series aluminium alloys have been shown to display atypical intergranular failure when in microcellular form [22, 23] and local strut or cell wall properties have been found to differ from those of the same alloy in dense form [23, 24]; fine-scale replicated microcellular Al-4.5wt%Cu was shown to solidify and respond to ageing differently to the bulk alloy when the pore size falls below roughly 100 μm [15, 25]; and since brittle second phases are frequently located near strut surfaces in microcellular alloys [17, 20, 26, 27], internal damage accumulates differently during deformation in a microcellular structure than it does in the same alloy in bulk form .

Here, we examine whether the flow stress of replicated Al-4.5wt%Cu displays the same relation between microstructure and flow stress as it does in the dense alloy. Al-4.5wt%Cu is a classical model alloy in metallurgical studies: it falls within a simple eutectic phase diagram, has been extensively studied from the standpoints of solidification, age-hardening and mechanical behaviour, and counts among the stronger cast engineering aluminium alloys [28, 29]. We vary its microstructure by producing the material at two different solidification rates and test the material in compression both before and after age-hardening, to explore how microstructural features affect the scaling relation between relative density (or porosity) and the flow stress of the material.

2. EXPERIMENTS

Open-cell foams of aluminium alloyed with 4.5wt% copper (containing 0.041wt% Fe and 0.022wt%Si, produced by Alusuisse in Neuhausen) were prepared by replication processing, as described in Refs. [1, 25, 30-32]. In brief, sieved monodisperse sodium chloride powder (99.5 % purity NaCl from Fluka Chemie GmbH, Buchs, Switzerland) with particles 400 μm in average diameter was packed and cold isostatically pressed under pressures in the range 30-45 MPa. These preforms were then infiltrated with molten Al-4.5wt%Cu under argon gas at 0.4 MPa, and then solidified under one of two conditions. The first, higher, cooling rate condition (hereafter designated as Condition A) corresponds to directional solidification of the NaCl/Al-4.5wt%Cu composite over a copper chill, resulting in a cooling rate ranging from -30 to -22 °/min (depending on distance from the chill). The second, lower, cooling rate (Condition C), corresponds to a much slower, homogeneous, cooling of the NaCl/Al-4.5wt%Cu composite within the furnace, at -0.5°C/min. The letters (A and C) correspond to those used in Ref. [25] to designate the same cooling conditions.

The solid Al-4.5wt%Cu/NaCl composites were machined into cylinders 10 mm in diameter and 10 mm high for subsequent compression testing. The salt was then leached in a chromate conversion solution made of 1.62 g/l Na_2CrO_4 and 0.84 g/l $NaHCO_3$ in distilled water ; this is a well-known corrosion inhibitor of aluminium in brine, used here to prevent aluminium hydroxide formation [33]. The resulting open-pore microcellular alloy samples have a relative density, V_m, situated at a prechosen and constant value between 0.12 and 0.25. Some samples were tested in the as-cast condition, while other samples were brought to the T6 condition by solution heat treatment at 525°C for 4 hours under argon, followed by quenching in water and age-hardening for 168h at 130°C under air. This heat treatment corresponds to peak of hardening of the alloy for this ageing temperature [15]. The four different microstructures tested are summarized in Table 1.

Compression testing was conducted using an MTS Alliance RT50 screw-driven testing machine, at a displacement rate of 5 μm/s (corresponding to a strain rate of 5 10^{-4} s^{-1}). The load was measured with a 5kN load cell. The strain was measured using three LVDTs fixed 120° apart around the bottom compression plate and recording the displacement of the upper plate. Young's Modulus $E_f(e)$ was determined using the slope of load-unload cycles performed at different values of the engineering strain e. The initial Young's modulus $E_{f,0}$ was determined by extrapolating the $E_f(e)$ curve to $e = 0$, as described in Ref. [6].

The mesostructure and the microstructure of the foam were examined by scanning electron microscopy (SEM) using a Philips XL 30 SEM operating at 15 kV and FEI Quanta Inspect 200LV equipped with EDAX, UTV detector and Genesis software. The metal microstructure was revealed by conventional metallographic preparation of porous or epoxy-infiltrated sections through samples of the microcellular alloy.

3. RESULTS

Figure 1 shows SEM micrographs in electron backscattered mode of the four different microcellular Al-4.5wt%Cu microstructures. The white phase corresponds to the θ (Al_2Cu) intermetallic and the light gray phase to primary α aluminium-copper solid solution. The as-cast microstructures obtained directly after infiltration (Conditions A and C) are shown on the left-hand side of Fig.1. As documented for similar samples in Ref.[25], when solidified more rapidly (Condition A) the as-cast microstructure is dendritic in wider portions of metal. In narrower metal struts of the foam, the eutectic tends to be located either along the free surface (the former NaCl/alloy interface), or in narrow bands that cross the strut, Fig. 2. In samples solidified more slowly (Condition C), the dendritic character of the solidified metal microstructure is lost, the level of microsegregation is strongly reduced, and essentially all intermetallic is located along the surface of the struts, as was shown in Ref. [25].

In both conditions one finds that the α + θ eutectic is visible along the pore surface, Fig. 1. A systematic examination of roughly twenty samples in the electron microscope revealed no noticeable difference between the microstructures across the range of values of relative density, V_m, explored here: the average copper concentration within the struts, the gradient in copper concentration along the struts, as well as the fraction of struts crossed by eutectic (roughly one-half), show no visible dependence on V_m.

The microstructures of the heat-treated samples (A+T6 and C+T6) are seen on the right-hand side of Fig.1: the amount of θ–phase is strongly reduced, while that portion which remains is coarser and primarily located along the pore surface. Thus, despite the solutionization treatment, intermetallics remain present.

After compression the Al-4.5wt%Cu foam shows traces of internal damage accumulation. This takes the form of cracking of intermetallic phases located along the foam surface, and of strut buckling. Examples are given in Fig. 3, which shows SEM micrographs of an as-cast sample after compression.

The foam Young's modulus $E_f(e)$ decreases as a function of the foam engineering strain e [6, 26, 30]. Figure 4 plots the initial Young's modulus, $E_{f,0}$, computed by extrapolation of $E_f(e)$ curves to e = 0 for each sample tested, versus foam relative density V_m. There is, as expected, no dependence on microstructure of the scaling law linking the modulus of the microcellular alloy with its relative density.

The rate of normalized stiffness decrease during compression, α, defined as:

$$\alpha = \frac{1}{E_{f,0}} \frac{dE_f}{de} \qquad (1)$$

averaged along each compression curve is an indicator of the rate at which internal damage accumulates within the foam as it deforms [26]. Figure 5 plots α for all four Al-4.5%Cu foam microstructures versus V_m. Similar data for 99.99% pure Al foams, from Ref. [34], are also plotted to show what obtains with a microstructure completely free of intermetallics. As seen, within the (significant) experimental scatter, no meaningful difference emerges between the four different alloyed foam structures, nor between these and microcellular pure aluminium.

Stress-strain curves of the microcellular alloy have the shape typical of replicated metal [1, 2] (see for example Fig. 4 of Ref. [6]). As is customary with microcellular materials [2, 3], the flow stress is a strong function of the relative density; this is seen in Fig. 6, which plots the flow stress of present samples at 3 or 5% compressive strain versus V_m. Also given in the figure are corresponding data for similarly processed and tested samples of 99.99% pure microcellular aluminium. The strong influence exerted by the relative density V_m on the flow stress is immediately apparent. Alloying and heat treatment also make a considerable difference, bringing the flow stress of the material in the same range as that of commercial aluminium-based foams, which have a better load-bearing (closed-cell) mesostructure than do replicated microcellular metals [2, 3]. Heat-treatment increases the flow stress by a factor near two, as was already reported in Ref. [15]; here again there is no visible systematic difference between the two solidification conditions.

4. DISCUSSION

4.1. Microstructure

As the alloy solidifies in the confined space between the NaCl particles, if cooling is slow the particles alter its microstructural development [25, 35]; this is observed here. Under Condition A the microstructure is dendritic, with coring and interdendritic eutectic: it resembles that which would be found, at similar cooling rates, in the bulk alloy. At the lower solidification speed, Condition C, the dendritic character is lost. This is due to accelerated dendrite arm coalescence caused by the (NaCl) reinforcement. Simultaneously, microsegregation is strongly reduced by diffusion in the constrained solid α-phase. Present observations are consistent with earlier results on this system; we refer to Refs. [25, 35] for a detailed discussion and explanation of this microstructure.

When the Al-4.5%Cu foams are heat-treated to the T6 state, most of the θ phase is dissolved; however, a certain fraction of intermetallic remains along the foam pore surfaces. That some residual intermetallic phase remain in the T6 microstructures, despite the high-temperature solutionisation heat treatment, is explained by the presence of iron impurities in the alloy. These form the essentially insoluble Al_7Cu_2Fe phase, which remains after solutionization in the microcellular alloy, as was documented in earlier work [15].

4.2. Mechanical properties

The evolution of $E_{f,0}$ (Fig. 4) as a function of V_m follows a power law scaling relation $E_{f,0} \alpha V_m^N$ with $N \approx 2.6$. This is consistent with earlier studies of replicated aluminium foam over this range of relative density values [6, 30, 36]. Such consistency is expected: the elastic stiffness of metals and alloys is a relatively microstructure-independent property.

The flow stress of Al-4.5%Cu foams is essentially doubled after age-hardening, as was already reported in Ref. [15]. The solidification rate has on the other hand essentially no influence on the flow stress of these open-cell foams. For the age-hardened foams this is reasonable, as the heat-treatment homogenises the microstructure, erasing to a large extent the effect of solidification conditions. The result is on the other hand more surprising for the as-cast microstructures, given that the two solidification speeds produce markedly different microstructures (Fig. 1). Differences in coring level, different amounts of θ-phase, and a difference in their scale or distribution thus apparently exert, in this system at least, little influence on the flow stress of the microcellular alloy.

4.3. Damage

All four Al-4.5wt%Cu foams present a rate of stiffness loss, α, that is similar, within experimental error, to that of pure Al replicated foams, Fig 5. This evolution of α is unlike that in replicated Al-12Si foam, which shows $\alpha \approx 10$ as a result of silicon particle cracking [26], or in Al-6.4wt%Ni foam, for which α is again measurably above data for pure Al [37].

That α not exceed in Al-4.5wt%Cu foams the value measured with pure Al is *a priori* surprising, since this alloy too contains brittle intermetallics ($\theta{-}Al_2Cu$ and Al_7Cu_2Fe), which fracture during foam deformation. The explanation is likely linked with the fact that $\theta{-}Al_2Cu$ and Al_7Cu_2Fe are mostly present as discrete islands along the pore surface (Figs. 1 and 3). The fraction of applied load carried by the intermetallic is therefore far lower than in Al-12%Si or Al-Ni alloy foams, where brittle second phases are more continuous and represent a higher volume fraction of the microstructure. Intermetallic fracture having apparently no noticeable influence on α, the rate of stiffness loss in Al-4.5wt%Cu foams is thus by the same mechanisms as in pure Al replicated foams, namely bending and buckling of struts, Fig. 3 [6, 30].

4.4. Scaling of the flow stress

The variational estimate of Ponte-Castañeda and Suquet [38-43], adapted and simplified for the monotonic uniaxial deformation of (incompressible) non-linear microcellular materials [6, 44, 45], allows an estimation of the *in-situ* stress-strain curves of the metal within the foams, knowing the relative density V_m, the Young's modulus scaling law, and the uniaxial flow curve of the microcellular metal. The calculation is detailed in Appendix A.

Figure 7(a) shows tensile curves measured on five samples of pure aluminium foam, produced by the same replication process as alloyed samples of this work and tested similarly. Figure 7(b) shows the back-calculated *in-situ* stress-strain cuves of the (pure Al) metal within these samples: as seen, the variational estimate collapses stress-strain curves of the five variously dense microcellular metal samples (Fig. 7a) into a single curve (Fig. 7b). This collapsed curve is, according to the model, the effective (von Mises) back-calculated *in-situ* stress-strain curve of the metal making the foam – with the caveat that it is likely scaled down by a fixed "knock-down" factor on the order of two to three, which has often been found in confronting data with theory but remains so far essentially unexplained [2, 6, 46, 47].

Save for this factor, the variational estimate thus provides a credible predictor of the scaling between the flow stress and the relative density of a replicated microcellular metal having a simple, essentially featureless, microstructure. It also performs well when confronted with steady-state creep data of replicated microcellular metal, as shown elsewhere [37, 48, 49].

Predictions of the model for the flow stress of the alloy are shown in Fig. 8. This plots the similarly back-calculated *in-situ* flow stress of replicated microcellular Al-4.5 wt%Cu at 3% (Fig. 8a) or 5% (Fig. 8b) strain, together with the corresponding values for the pure Al samples.

The back-calculated flow stress for pure Al is single-valued across all values of V_m, consistent with Fig. 7 and the fact that the variational model accounts well for the observed scaling behaviour of the flow stress. It varies somewhat more but still remains relatively constant for heat-treated (T6) microcellular Al-4.5wt%Cu when $V_m \geq 20\%$: the back-calculated *in-situ* flow stress is within the ranges 130-160 MPa at $\varepsilon_{eff} = 3\%$, 140-170 MPa at $\varepsilon_{eff} = 5\%$, Fig. 8. Note that these values are lower than the flow stress measured on dense castings of heat-treated Aluminium Alloy 201, of similar nominal composition 4.6wt%Cu-0.7wt%Ag-0.35wt%Mn-0.35wt%Mg-0.25wt%Ti [29], which is in the range of 250 to 450 MPa after peak hardening [50]. This difference in flow stress, by a factor near two, is likely another example of the frequently reported "knock-down" factor between theory and data for the plastic flow stress of microcellular materials [2, 6, 46, 47].

In other samples the back-calculated flow stress decreases with decreasing relative density. It falls below 100 MPa for the two heat-treated samples when $V_m \approx 0.1$, and it decreases steadily with decreasing V_m for as-cast samples in both A and C conditions. Thus, the scaling relation that is predicted by the variational estimate is not obeyed by the alloyed metal in microcellular samples produced and tested here. This implies that their microstructure causes an additional dependence of the flow stress on relative density.

One potential cause for this was already mentioned in Ref. [6], namely internal damage. In applying the variational estimate, F (Eq. A5) was estimated on the basis of the *initial* Young's modulus of the foam, $E_{f,0}$, for two reasons: (i) the variational estimate is restricted to small-strain deformation and (ii) it is valid only for isotropic materials (the foam becomes anisotropic after significant deformation). In reality E_f decreases with e at a rate that is measured by the damage parameter α (Eq. 1, Fig. 5). Looking at Eqs. (A6) and (A8) one sees that an overestimation of E_f, and hence of F, by a factor X (X>1), will cause an underestimation of the back-calculated *in-situ* metal flow stress σ_{eff} by a factor on the order of $X^{-1/2}$ (while the corresponding *in-situ* strain ε_{eff} is overestimated by a factor on the order of $X^{1/2}$, Appendix A). Since $X \approx (1-\alpha\, e)^{-1}$, this causes the *in-situ* metal flow stress to be underestimated by a factor on the order of $(1-\alpha\, e)^{1/2}$. At small strain and with α values in Fig. 5, the resulting error is on the order of a few percent; however, for, say, e = 10% and α = 5, then X = 2 and the flow stress is underestimated by a factor on the order of $\sqrt{2}$ (the theory being, besides, outside of its range of validity [2, 6, 45, 51]). At high α, therefore, internal damage offers one explanation for lower-than-expected back-calculated *in-situ* alloy flow curves. Since α increases as V_m falls near 0.1 (Fig. 5; see also Fig. 8 of Ref. [37]), accelerated damage might contribute an explanation to the lower *in-situ* flow stresses back-calculated for heat-treated microcellular Al-4.5wt%Cu when $V_m \approx 0.1$.

This however does not explain why the *in-situ* flow stress of the metal within the as-cast Al-4.5%Cu foams varies monotonically with V_m, Fig.7: α values are too low for this. Also, α is similar for pure Al or the alloy in all conditions; were it the cause for the observed decrease in apparent *in-situ* flow stress for decreasing V_m, then pure Al and T6 alloy data should be similarly affected. This is not observed (Fig. 8). So there must be another cause for the decreasing *in-situ* as-cast alloy flow stress with decreasing V_m.

The key difference between the metal in as-cast microcellular Al-4.5wt%Cu on one hand, and Al-4.5wt%Cu in the T6 condition or pure Al on the other, is the heterogeneity of the as-cast alloy microstructure, for both cooling conditions: coring and second phases are present in the as-solidified alloy microstructure and are removed after heat-treatment, or are absent in the pure metal. As mentioned above, no systematic variation with V_m could be found in the microstructure of the solidified metal within the foams: the nature, size, and distribution of phases are visibly the same, as are concentration gradients (these were estimated in several samples of different V_m using energy-dispersive X-ray analysis in the scanning electron microscope). In short, despite extensive investigation, no evolution of the microstructure could be found that would explain why the *in-situ* metal flow stress decreases as V_m decreases.

We propose that the answer lies in the fact that, as V_m decreases with the alloy microstructure unchanged, the struts become thinner. This may cause the strut flow stress to evolve, since the nature and length-scale of the alloy microstructure remain constant and are commensurate in size with the strut width (a few μm). Indeed, if there are certain regions of the matrix microstructure that are weaker than the rest, then as V_m decreases, each weak region will locally represent a greater fraction of the strut cross section, and hence cause a greater local weakening of the material wherever it appears.

Such weak regions are unlikely to be the brittle second phase θ, given that Young's modulus of the foams would also be affected (Fig. 5). Rather, these must be regions with a lower flow stress but a modulus that remains near that of the metal. A likely culprit is the band of solute-poor metal that lines larger intermetallic phases; Fig. 9 shows such bands (a) within the microcellular alloy in a node, and (b) within a portion of the strut shown in Fig. 2(b). These are well-known (colour metallography reveals them well in Fig. 3 of Ref. [52]) and appear because, while Al-4.5wt%Cu cools below the eutectic temperature, the solubility limit of copper within the primary α-phase decreases. Kinetics permitting, the amount of Al_2Cu intermetallic therefore increases as the alloy cools. This occurs either by diffusion and deposition of copper atoms onto existing (eutectic) θ-phase, or alternatively by nucleation and growth of new Al_2Cu, often visible as θ' platelets within the primary α-phase of the cast alloy. In the proximity of eutectic Al_2Cu, the former mechanism prevails, while further away from eutectic Al_2Cu the latter mechanism dominates. The result is a band of softer precipitate-free copper-poor alpha-phase lining the eutectic θ-phase, the remainder of the alpha-phase containing a distribution of θ' platelets; such bands are shown in Fig. 9.

What this implies is that much of the surface of metal struts is lined with a band of copper-deplected (and hence softer) α-phase. Now the thickness of this band, on the order of a few micrometres (Fig. 9), is governed by the alloy cooling rate; it is independent of the strut thickness. As V_m decreases, and with it the average thickness of struts within the microcellular material, such copper-depleted bands therefore represent an increasing proportion of the local struts cross-section, which can explain in turn why the apparent average *in-situ* flow stress decreases as V_m decreases. The bands exist after both A and C cooling conditions; it is hence reasonable that their effect be similar. After homogenization, alpha-phase concentration gradients are mostly erased, and these solute-poor bands are removed: this explains why there is much less of a spread with V_m in apparent metal *in-situ* flow curves after heat-treatment, Fig. 8.

The more general implication is that the flow stress of microcellular metals (or materials more generally) can show unexpected scaling of their flow stress with relative density when the dimensional scale of pores (the mesostructure) and that of microstructural features within the base material (the microstructure) are commensurate. If the two do not scale similarly as the relative density changes, or if one is not much finer than the other, then the average *in-situ* flow stress of the metal within the foam can vary with V_m, affecting in turn the scaling between relative density and strength for the microcellular metal.

In closing, we note that the effect shown here (i) has a parallel in the interplay between microstructure, mesostructure and strength that emerges from simulations of fracture in 2D microcellular structures by Mangipudi and Onck [53] and (ii) that it can be viewed as a manifestation of percolation size effects in the mechanical flow of materials: this is illustrated in Appendix B with a simple two-dimensional model.

5. CONCLUSIONS

- Replicated 400µm pore size Al-4.5%Cu foam solidified at one of two cooling conditions is tested in compression in the as-cast and age hardened (T6) condition. At given relative density V_m the yield strength is unaffected (within uncertainty) by the solidification rate; it increases by a factor near two after age-hardening.
- Brittle intermetallic phases (Al_2Cu and Al_7Cu_2Fe) are present in the two as-cast microstructures but are mostly dissolved after heat-treatment. Intermetallic phases are predominantly located along the foam pore surface. These fracture during foam compression; however, this does not influence the rate of Young's modulus decrease with foam strain.
- The *in-situ* flow stress of the metal within the foams, back-calculated using the variational estimate knowing their modulus and the relative density V_m, is consistent for heat-treated Al-4.5%Cu when $V_m \geq 0.2$, as is found also for pure Al. With as-cast Al-4.5%Cu in both conditions the apparent average *in-situ* metal flow stress increases with increasing V_m. We propose that this is caused by the presence of a band of copper-depleted α–phase along the interface with intermetallics in the as-cast foam alloy, the thickness of these bands remaining constant while the strut thickness decreases with decreasing V_m.
- When microstructural features of microcellular materials are of a size scale commensurate with that of their mesostructure, the scaling between relative density and flow stress can be altered compared to what obtains for a uniform elastoplastic continuum.

APPENDIX A – Estimating the metal *in-situ* flow curve from that of the foam knowing its Young's modulus, according to the simplified variational estimate

Assume that dislocation motion in the metal is governed by the second order moment of the instantaneous stress field in the metal making the foam, σ_{eff}. The rationale behind this assumption is that (i) the Von Mises stress is the simplest scalar measure of stress driving dislocation motion in complex three-dimensional stress fields and (ii) σ_{eff} is used, in the variational estimate, to deduce the appropriate matrix secant modulus that serves to derive the instantaneous non-linear deformation state in the metal making the foam [42, 43].

The variational estimate gives σ_{eff} from the volumetric average of the second order moment of the stress field in the linear comparison cellular material, which itself is related to the foam compliance M_{e} by [42, 43]:

$$\sigma_{\mathrm{eff}} = \left\{ \frac{3}{V_{\mathrm{m}}} \left[s^* : \left(\frac{\partial M_e}{\partial \left(1 / G_{\mathrm{m}} \right)} \right)_{G_{\mathrm{m}} = G_{\mathrm{ms}}} : s^* \right] \right\}^{1/2} \tag{A1}$$

where s^* is the instantaneous uniaxial stress applied monotonically to the porous foam material and G_{m} is the (dense) metal shear modulus. Volume changes of plastically deforming materials are very small and high average hydrostatic stresses are unlikely in the matrix of a porous material: as in Ref.[6], we therefore assume that the metal matrix behaves as if it were incompressible. For uniaxial tensile deformation, Eq. (A1) then simplifies to:

$$s^* = \sqrt{\frac{1 - V_{\mathrm{p}}}{3a}} \cdot \sigma_{\mathrm{eff}} = \sqrt{\frac{V_{\mathrm{m}}}{3a}} \cdot \sigma_{\mathit{eff}} \tag{A2}$$

with

$$a = \left(\frac{\partial \left(1 / E_{\mathrm{f}} \right)}{\partial \left(1 / G_{\mathrm{m}} \right)} \right)_{G_{\mathrm{m}} = G_{\mathrm{ms}}} \tag{A3}$$

where G_{ms} is the secant shear modulus of the material making the foam at the relevant point of deformation of the foam. This is related to the secant Young's modulus E_{ms} of the (incompressible, dense) material by:

$$E_{\mathrm{ms}} = \frac{\sigma_{\mathrm{eff}}}{\varepsilon_{\mathrm{eff}}} = 3 G_{\mathrm{ms}} \tag{A4}$$

where $\varepsilon_{\mathrm{eff}}$ is the average equivalent strain that corresponds, according to the monotonic constitutive law of the material making the foam (in Von Mises terms its tensile uniaxial stress-strain curve), to the instantaneous value of σ_{eff} [54]. Now, the foam Young's modulus E_{f} is, for the given (isotropic) porous material mesostructure, equal to a certain fraction, F, of the Young's modulus E_{m} of the solid material making the foam:

$$E_{\text{f}} = F\,E_{\text{m}} \tag{A5}$$

where F is an increasing function of the relative density V_{m} of the foam. This being the case, Eq. (A2) implies

$$\sigma_{\text{eff}} = \frac{s^*}{\sqrt{F_{(V_{\text{m}})}V_{\text{m}}}}\,. \tag{A6}$$

By definition of the secant modulus E_{fs} of the deforming foam:

$$e^* = \frac{s^*}{E_{\text{fs}}} = \frac{s^*}{F_{(V_{\text{m}})}E_{\text{ms}}} = \frac{\sqrt{F_{(V_{\text{m}})}V_{\text{m}}}}{F_{(V_{\text{m}})}}\frac{\sigma_{\text{eff}}}{E_{\text{ms}}} = \sqrt{\frac{V_{\text{m}}}{F_{(V_{\text{m}})}}}\varepsilon_{\text{eff}} \tag{A7}$$

where ε_{eff} is the matrix equivalent strain corresponding to the current equivalent stress, σ_{eff}, in the matrix (Eq. A1).

Therefore, if one plots, knowing the stress-strain curve (s^*, e^*) of the microcellular material, σ_{eff} as given in Eq. (A6) versus

$$\varepsilon_{eff} = e^*\sqrt{\frac{F_{(V_{\text{m}})}}{V_{\text{m}}}}\,, \tag{A8}$$

then one recovers the monotonic stress-strain curve of the material making the foam, as estimated (under its assumptions) by the modified secant modulus method that corresponds to the variational estimate of Ponte-Castañeda and Suquet coupled with assumptions made above. For the present foams, from experimental data we have $F = 1.62 \cdot V_m^{2.61}$ (Fig. 4). Note that the above theory and hence the estimated stress-strain curves are strictly only valid for isotropic materials under small strain deformation. The back-calculated curves are therefore strictly only valid at low values of e or ε_{eff}.

APPENDIX B – Illustrating how percolation size effects intervene when mesostructural and microstructural length scales are commensurate

Consider a strut in a foam made of a heterogeneous metal that is composed of softer zones and harder zones. At fixed pore size, when the relative density varies, the greatest change in mesostructure is that the struts making the foam become thinner. Assume a two-dimensional strut, separated into a checkerboard assembly of rectangular elements, *N* elements across the width and *M* elements along the length of the beam, as schematized in Fig. B-1. Each rectangular element is either soft or hard, with *P* the probability for an element to be soft. The shear flow stress τ as a function of shear strain γ in any given element is taken to be either:

$$\tau_i = \tau_{y,1} + \alpha_1 \gamma \quad \text{with probability } P \tag{B-1}$$

or:

$$\tau_i = \tau_{y,2} + \alpha_2 \gamma \quad \text{with probability } (1-P) \tag{B-2}$$

with $\tau_{y,1}$ the yield shear stress and α_1 the strain hardening coefficient of the soft elements, and $\tau_{y,2}$ and α_2 the yield shear stress and strain hardening coefficient of the hard elements. For argument's sake, we give soft elements the values corresponding to binary Al-1%Cu, namely $\tau_{y,1}$ = 35 MPa and α_1= 100 MPa, while for the hard elements we take values typical of binary Al-4%Cu, namely $\tau_{y,1}$ = 100 MPa and α_1= 750 MPa [28].

We simplify loading of the beam as simple shear with the volume elements arranged as equal rectangles on a regular grid. We make the (simplistic) assumption that deformation of the beam occurs by isostrain deformation across the beam and isostress deformation along the beam, as the assumed geometry suggests (Fig. B-1). The average shear stress τ_j in line *j* at shear strain γ_j is then given by:

$$\tau_j = \sum_{i=1}^{N} \frac{\tau_{y,i}}{N} + \frac{\alpha_i}{N}\gamma_j \tag{B-3}$$

if there are *N* elements across. This gives for γ_j, after rearrangement:

$$\gamma_j = \frac{N\tau_j - \sum_{i=1}^{N}\tau_{y,i}}{\sum_{i=1}^{N}\alpha_i}. \tag{B-4}$$

The average shear strain γ of the whole strut is then:

$$\gamma = \sum_{j=1}^{M} \frac{1}{M}\left[\frac{N\tau - \sum_{i=1}^{N}\tau_{y,i}}{\sum_{i=1}^{N}\alpha_i}\right], \tag{B-5}$$

if it is M elements long.

Calculations were conducted using a simple spreadsheet; the evolution of γ with the width of this fictive 2D strut is given in Fig. B-2 for $\tau = 110$ MPa. The results correspond to an average over 20 struts with randomly generated elements for the relevant value of P. The bold line corresponds to the mean value of γ, and the thin lines show the standard-deviation for the strain to which a single such 2D checkerboard beam will deform under $\tau = 110$ MPa. As seen, at high values of N, *i.e.*, for thicker struts (high V_m), the values converge to a constant value, corresponding to an averaging over a large number of "typical" random elements. For low values of N, *i.e.*, for thinner struts (low V_m), γ tends to increase. This indicates a softening of the struts, or in other words a lowering of the average strut (and hence of the foam) flow stress. These trends are caused by the increased probability for soft zones to percolate across the width of thinner struts, which softens the entire beam at fixed phase proportions.

Figure B-2 is drawn for two values of the probability P for the presence of a soft zone; one with a higher probability, $P = 0.5$ (to illustrate the as-cast structures, which contain a higher proportion of heterogeneity) and one with $P = 0.1$ to simulate the T6 microstructures (which have fewer sites of heterogeneity). As seen, for the same range of variation of the strut thickness (*i.e.*, the same range of V_m values), one finds (i) a plateau, and then softening only at the lower end of the strut thickness range (and hence for the lowest V_m) in the material with fewer soft zones, and (ii) a regular decrease of the flow stress in the material with a greater proportion of softer regions. This simple model can thus reproduce quite faithfully all trends observed in the present experimental data (Fig. 8).

ACKNOWLEDGMENTS

This work was funded by the Swiss National Science Foundation, Project No. 200020-100179/1.

6. REFERENCES

[1] Y Conde, JF Despois, R Goodall, et al. (2006) Advanced Engineering Materials 8: 795-803.

[2] R Goodall, A Mortensen (2013) in Hono K, Laughlin D (eds)Physical Metallurgy: 5th EditionElsevier, Amsterdam, NL

[3] MF Ashby, A Evans, NA Fleck, LJ Gibson, JW Hutchinson, HNG Wadley (2000) Metal Foams: A Design Guide. Butterworth Heinemann, Boston USA,

[4] C Tekoglu, LJ Gibson, T Pardoen, PR Onck (2011) Progress in Materials Science 56: 109-138. Doi:10.1016/j.pmatsci.2010.06.001

[5] HNG Wadley (2006) Philosophical Transactions of the Royal Society A: Mathematical, Physical and Engineering Sciences 364: 31.
[6] JF Despois, R Mueller, A Mortensen (2006) Acta Materialia 54: 4129-4142.
[7] D Lehmhus, C Marschner, J Banhart, H Bomas (2002) J Mater Sci 37: 3447-3451. Doi:10.1023/a:1016506905271
[8] D Lehmhus, J Banhart (2003) Materials Science and Engineering A 349: 98.
[9] Y Feng, N Tao, Z Zhu, S Hu, Y Pan (2003) Materials Letters 57: 4058-4063.
[10] J Zhou, Z Gao, AM Cuitino, WO Soboyejo (2004) Materials Science and Engineering A 386: 118-128.
[11] J Zhou, WO Soboyejo (2004) Materials Science and Engineering A 369: 23-35.
[12] XQ Cao, ZH Wang, HQ Ma, LM Zhao, GT Yang (2006) Transactions of Nonferrous Metals Society of China 16: 159-163. Doi:http://dx.doi.org/10.1016/S1003-6326(06)60028-9
[13] E Amsterdam, JTM De Hosson, PR Onck (2008) Advanced Engineering Materials 10: 877-881. Doi:10.1016/j.scriptamat.2008.05.025
[14] E Amsterdam, JTM De Hosson, PR Onck (2008) Scripta Materialia 59: 653-656. Doi:10.1016/j.scriptamat.2008.05.025
[15] Y Conde, A Mortensen (2008) Advanced Engineering Materials 10: 849-852. Doi:10.1002/adem.200800086
[16] DA Cluff, S Esmaeili (2008) J Mater Sci 43: 1121-1127. Doi:10.1007/s10853-007-2271-9
[17] F Campana, D Pilone (2009) Scripta Materialia 60: 679-682. Doi:http://dx.doi.org/10.1016/j.scriptamat.2008.12.045
[18] Z Wang, Z Li, J Ning, L Zhao (2009) Materials & Design 30: 977-982. Doi:http://dx.doi.org/10.1016/j.matdes.2008.06.058
[19] PH Thornton, CL Magee (1975) Metallurgical Transactions 6A: 1253-1263.
[20] Y Yamada, K Shimojima, Y Sakaguchi, et al. (2000) Materials Science and Engineering A280: 225-228.
[21] H Kanahashi, T Mukai, Y Yamada, et al. (2001) Materials Science and Engineering A308: 283-287.
[22] E Amsterdam, PR Onck, JTM De Hosson (2005) J Mater Sci 40: 5813.
[23] J Zhou, A S., WO Soboyejo (2005) J Mater Sci 40: 429-439.
[24] I Jeon, K Katou, T Sonoda, T Asahina, K-J Kang (2009) Mechanics of Materials 41: 60-73. Doi:http://dx.doi.org/10.1016/j.mechmat.2008.08.002
[25] Y Conde, A Mortensen (2010) Met. Mater. Trans. A 41: 2048-2055.
[26] C San Marchi, JF Despois, A Mortensen (2004) Acta Materialia 52: 2895-2902.
[27] SF Fischer, P Schüler, C Fleck, A Bührig-Polaczek (2013) Acta Materialia 61: 5152-5161. Doi:http://dx.doi.org/10.1016/j.actamat.2013.04.069
[28] LF Mondolfo (1976) Aluminum Alloys: Structure and Properties. Butterworths, London
[29] JR Davis (ed) (1998) Metals Handbook, Desk Edition - Second Edition. ASM International, Metals Park, OH
[30] C San Marchi, A Mortensen (2001) Acta Materialia 49: 3959-3969.
[31] C San Marchi, A Mortensen (2002) in Degischer HP, Kriszt B (eds)Handbook of Cellular MetalsWiley-VCH Verlag, Weinheim Germany,
[32] JF Despois, A Marmottant, Y Conde, et al. (2006) Materials Science Forum 512: 281-288.
[33] F Diologent, R Goodall, A Mortensen (2009) Acta Materialia 57: 286-294.
[34] J-F Despois (2005) EPFL Thesis number 3268, Institute of Materials, Ecole Polytechnique Fédérale de Lausanne, Lausanne, Switzerland.

[35] A Mortensen, MC Flemings (1996) Metallurgical and Materials Transactions 27A: 595-609.
[36] R Goodall, A Marmottant, L Salvo, A Mortensen (2007) Materials Science and Engineering: A 465: 124-135. Doi:10.1016/j.msea.2007.02.002
[37] F Diologent, Y Conde, R Goodall, A Mortensen (2009) Philosophical Magazine 89: 1121-1139.
[38] P Ponte-Castañeda (1991) Journal of the Mechanics and Physics of Solids 39: 45-71.
[39] JC Michel, PM Suquet (1992) Journal of the Mechanics and Physics of Solids 40: 783-812.
[40] PM Suquet (1993) Journal of the Mechanics and Physics of Solids 41: 981-1002.
[41] PM Suquet (1995) Comptes Rendus de l'Académie des Sciences de Paris 320: 563-571.
[42] P Suquet (1997) in Suquet P (ed)Continuum MicromechanicsSpringer-Verlag, Wien, New York
[43] P Ponte-Castañeda, P Suquet (1998) Advances in Applied Mechanics 34: 171-302.
[44] R Mueller, A Mortensen (2006) Acta Materialia 54: 2145.
[45] R Mueller, S Soubielle, R Goodall, F Diologent, A Mortensen (2007) Scripta Materialia 57: 33.
[46] LJ Gibson, MF Ashby (1997) Cellular Solids - Structure and Properties - Second Ed. Cambridge University Press, Cambridge, U.K.
[47] F Diologent, R Goodall, A Mortensen (2011) Acta Materialia 59: 6869-6879. Doi:10.1016/j.actamat.2011.07.021
[48] F Diologent, R Goodall, A Mortensen (2009) Acta Materialia 57: 830.
[49] S Soubielle, F Diologent, L Salvo, A Mortensen (2011) Acta Materialia 59: 440-450. Doi:10.1016/j.actamat.2010.09.037
[50] C Moosbrugger (ed) (2002) Atlas of Stress-strain curves. ASM International, Materials Park OH, USA
[51] KR Mangipudi, SW van Buuren, PR Onck (2010) International Journal of Solids and Structures 47: 2081-2096. Doi:10.1016/j.ijsolstr.2010.04.009
[52] A Mortensen, MN Gungor, JA Cornie, MC Flemings (1986) Journal of Metals 38: 30-35.
[53] KR Mangipudi, PR Onck (2011) Journal of the Mechanics and Physics of Solids 59: 1437-1461. Doi:10.1016/j.jmps.2011.02.008
[54] M Berveiller, A Zaoui (1978) Journal of the Mechanics and Physics of Solids 26: 325-344.

TABLES

Table 1: The four Al-4.5wt%Cu alloy processing conditions explored and their designation

Cooling condition	Condition A		Condition C	
Cooling Rate[°C/s]	-30 to-22		-0.5	
Solidification time t_f[s]	200 to 270		12,000	
Age Hardening	None	168h at 130°C (peak hardening)	None	168h at 130°C (peak hardening)
Designation	A	A+T6	C	C+T6

FIGURES

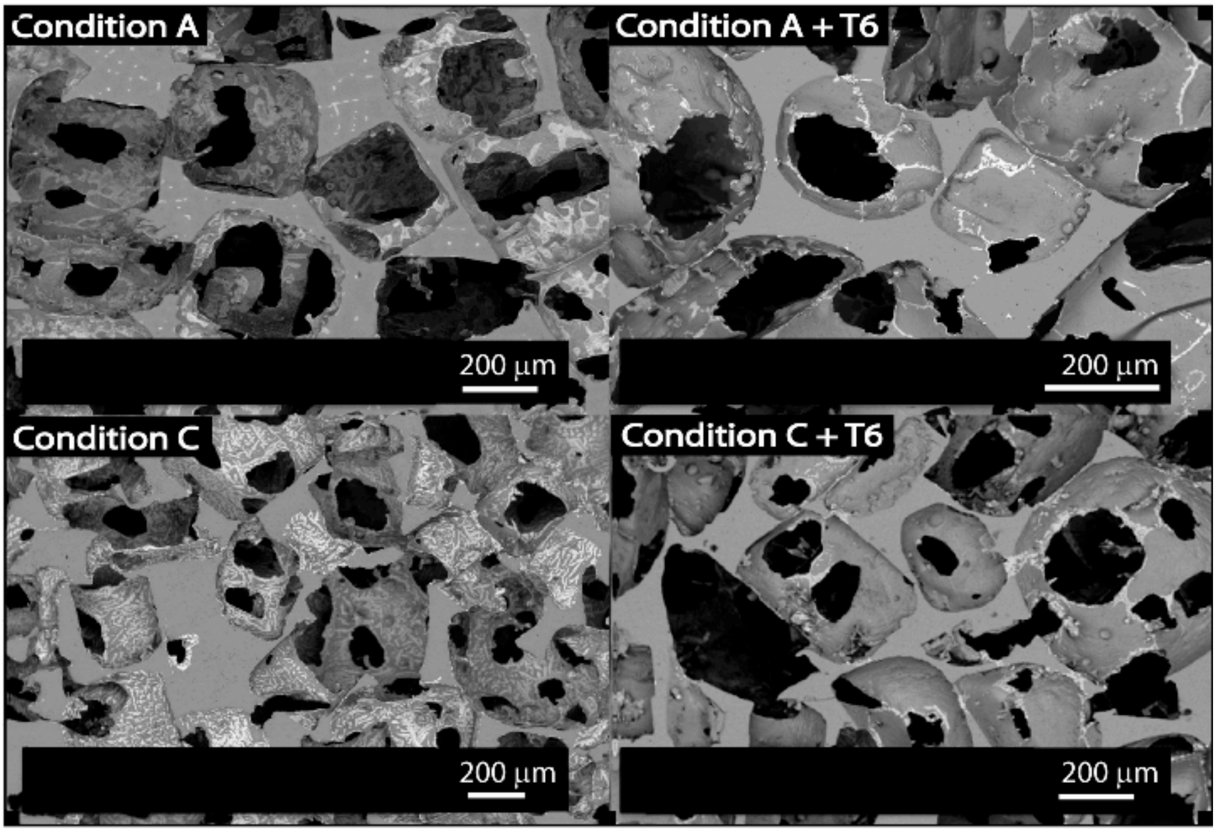

Figure 1: Microstructure of the four different Al-4.5%Cu foams. Top left (1): as-cast material solidified more rapidly (Condition A). Bottom left (2): as-cast material solidified slowly (Condition C). Top right (A+T6): heat-treated material solidified under Condition A. Bottom right (C+T6): heat-treated material solidified under Condition C.

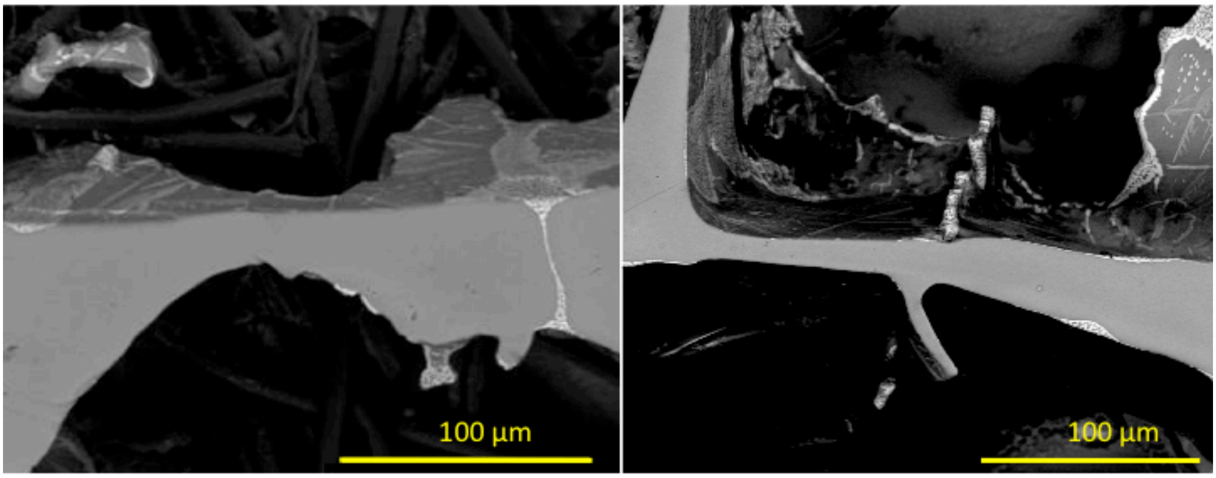

Figure 2 – Scanning electron micrographic close-ups of polished sections through individual struts in a non-deformed as-cast material of relative density 11% solidified more rapidly (Condition A); micrographs show the θ-phase located along the strut surface and, in one strut (left) crossing the strut.

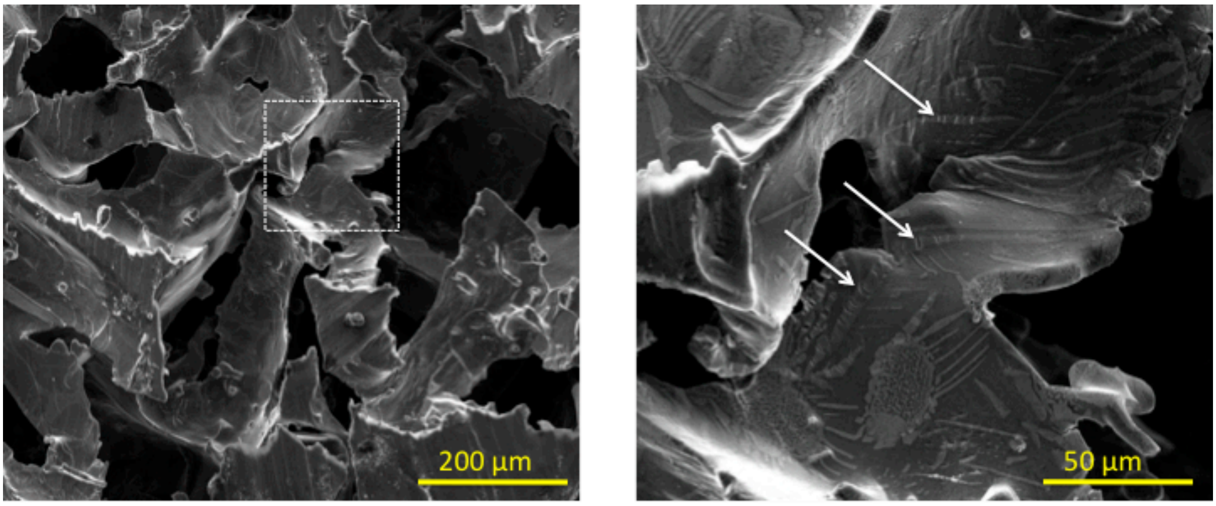

Figure 3: Secondary electron SEM micrograph of compressed as-cast Al-4.5wt%Cu (V_m = 11% deformed to 4% strain) showing (a, left) deformed struts along the sample surface and the marked area at higher magnification (b, right) showing evidence of internal damage by microcracking of the intermetallic θ-phase (indicated with white arrows) as well as strut buckling.

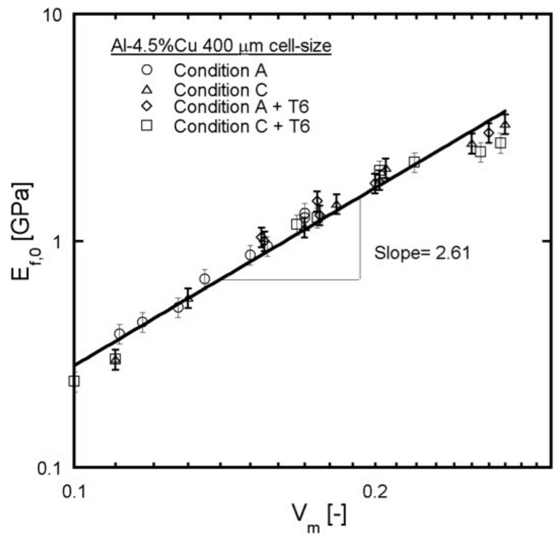

Figure 4: Evolution of Young's modulus $E_{f,0}$ as a function of the relative density V_m for Al-4.5%Cu foams with with both as-ast and T6 microstructures, for both cooling rates (Conditions A and C, Table 1). The log-log plot suggests a power-law relation of exponent near 2.6.

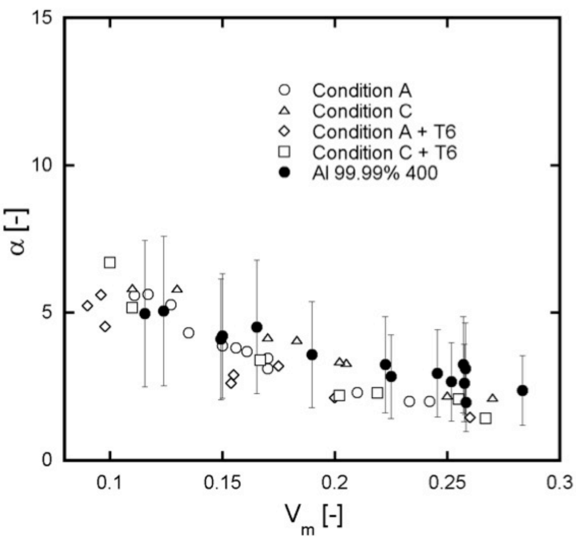

Figure 5: Evolution of the damage parameter a with the relative density V_m, for Al-4.5%Cu foams with as-cast and T6 microstructures; the evolution of a for pure Al foams (measured in earlier work) is also shown. The experimental error on a is approximately of 50%; for clarity, it is only shown on pure Al foams.

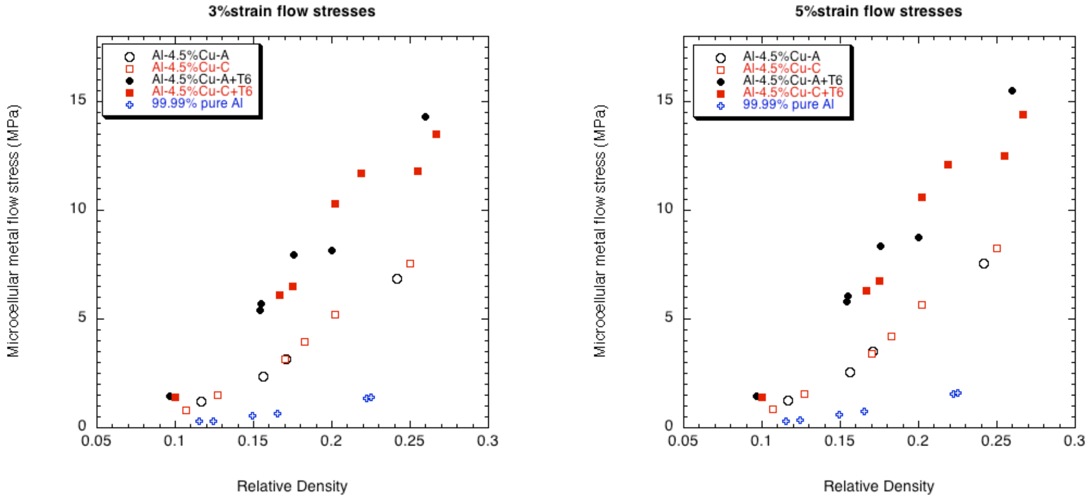

Figure 6: Flow stress of all tested microcellular samples at 3 % (a) or 5% (b) strain (in uniaxial compression) versus V_m. Also given in the figure are corresponding data for similarly processed and tested samples of 99.99% pure microcellular aluminium.

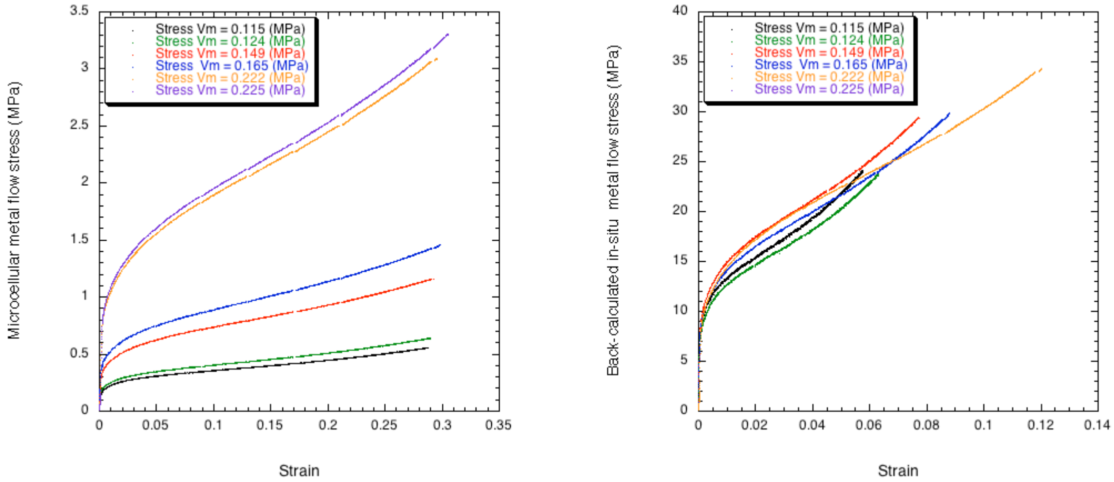

Figure 7: (a) Measured flow curves of replicated 400 µm pore size microcellular 4N pure aluminium; (b) back-calculated in-situ strain-stress curves for pure Al in these replicated foams (using the variational estimate)

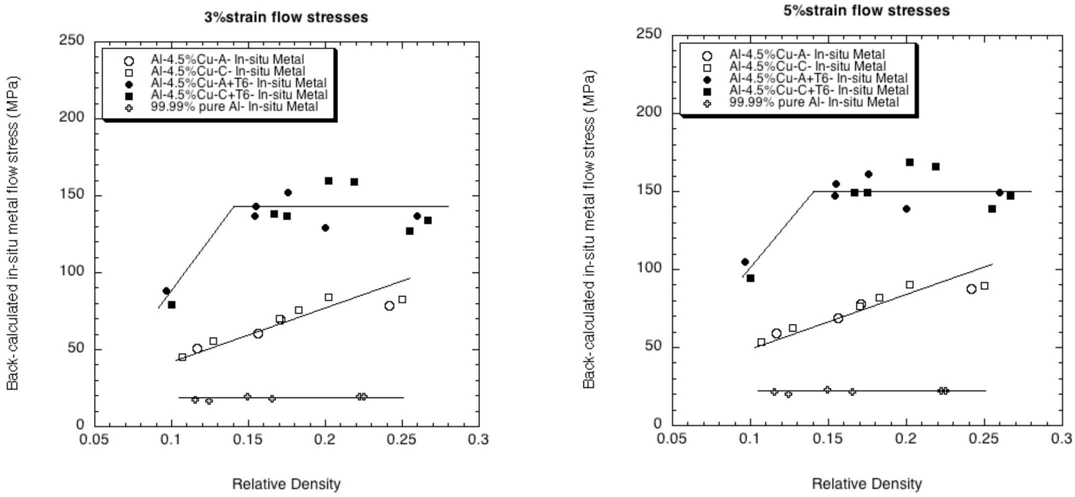

Figure 8: Back-calculated *in-situ* alloy flow stress in all tested microcellular samples at 3 % (a) or 5% (b) effective strain versus V_m. Also given in the figure are corresponding data for similarly processed, tested and analyzed samples of 99.99% pure microcellular aluminium (also given in Figs. 6 and 7).

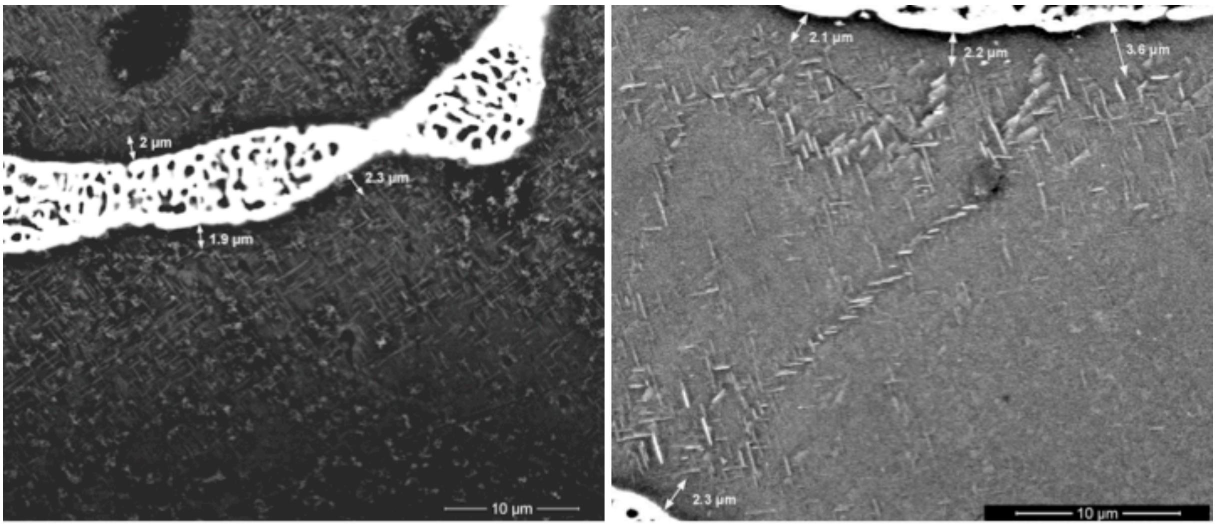

Figure 9: (a) back-scattered scanning electron microscopy image of as-cast Al-4.5wt%Cu within a node of foam having V_m = 0.17, cooled under Condition A revealing the eutectic θ-phase and precipitated θ' platelets (white) within the primary aluminium-rich α-phase (dark). (b) portion of the strut in Fig. 2b, showing θ' platelets within the α-phase. In both θ' platelets are essentially absent within a band roughly 3 µm wide lining the (white) eutectic θ-phase; the band is indicated with arrows in both micrographs.

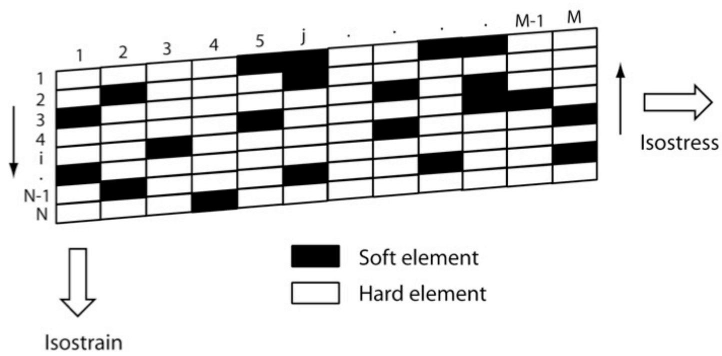

Fig. B-1: Two dimensional beam made of random rectangular patches of soft and hard materials, the former being present with probability *P*, the latter with probability (1-*P*).

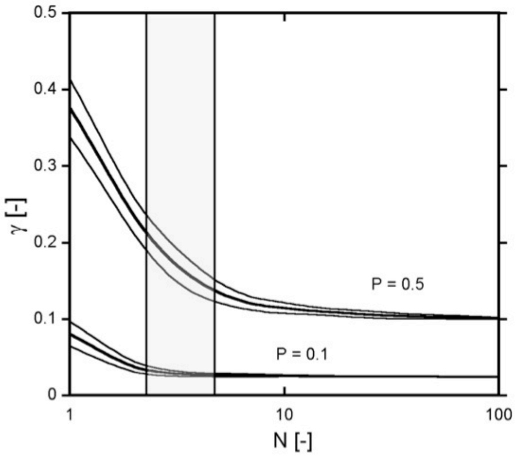

Fig. B-2: Deformation of the rectangular beam in Fig. B-1 at fixed applied stress versus its width (measured by the number of patches *N*) for two values of the soft phase probability *P*. Curves indicate the mean and standard deviation of 20 simulations for each condition.